AGU PUBLICATIONS

Geochemistry, Geophysics, Geosystems

RESEARCH ARTICLE
10.1002/2013GC005094

Magnetic properties and paleointensities as function of depth in a Hawaiian lava flow

Lennart V. de Groot[1], Mark J. Dekkers[1], Martijn Visscher[2], and Geertje W. ter Maat[1]

[1]Department of Earth Sciences, Paleomagnetic Laboratory Fort Hoofddijk, Utrecht University, Utrecht, Netherlands, [2]Neuroimaging Group, MIRA Institute for Biomedical Engineering and Technical Medicine, University of Twente, Enschede, Netherlands

Key Points:
- Rock-magnetic properties vary as function of depth in an inflated sheet flow
- These variations govern the chance of success in paleointensity experiments
- Calibrated pseudo-Thellier is an important new paleointensity technique

Supporting Information:
- Readme
- Figure S1, S2, S3
- Table S1

Correspondence to:
L. V. de Groot,
l.v.degroot@uu.nl

Citation:
de Groot, L. V., M. J. Dekkers, M. Visscher, and G. W. ter Maat (2014), Magnetic properties and paleointensities as function of depth in a Hawaiian lava flow, *Geochem. Geophys. Geosyst.*, *15*, 1096–1112, doi:10.1002/2013GC005094.

Received 15 OCT 2013
Accepted 24 FEB 2014
Accepted article online 27 FEB 2014
Published online 22 APR 2014

Abstract The outcome of paleointensity experiments largely depends on the rock-magnetic properties of the samples. To assess the relation between volcanic emplacement processes and rock-magnetic properties, we sampled a vertical transect in a ~6 m thick inflated lava flow at Hawaii, emplaced in ~588 AD. Its rock-magnetic properties vary as function of distance from the flow top; the observations can be correlated to the typical cooling rate profile for such a flow. The top and to a lesser extent the bottom parts of the flow cooled faster and reveal a composition of ~TM60 in which the magnetic remanence is carried by fine-grained titanomagnetites, relatively rich in titanium, with associated low Curie and unblocking temperatures. The titanomagnetite in the slower cooled central part of the flow is unmixed into the magnetite and ülvospinel end-members as evidenced by scanning electron microscope observation. The remanence is carried by coarse-grained magnetite lamella (~TM0) with high Curie and unblocking temperatures. The calibrated pseudo-Thellier results that can be accepted yield an average paleointensity of 44.1 ± 2.4 μT. This is in good agreement with the paleointensity results obtained using the thermal IZZI-Thellier technique (41.6 ± 7.4 μT) and a recently proposed record for Hawaii. We therefore suggest that the chance of obtaining a reliable paleointensity from a particular cooling unit can be increased by sampling lavas at multiple levels at different distances from the top of the flow combined with careful preliminary testing of the rock-magnetic properties.

1. Introduction

How the intensity of the Earth's magnetic field changes with time is presently rather poorly known. Direct observations have been made for the last 170 years; for older ages, we have to rely on well-dated materials that acquired their natural remanent magnetization (NRM) by cooling in the paleofield. The two most important recorders of the paleointensity are therefore burnt archaeological artifacts and extrusive igneous rocks. Due to often better-constrained ages and more favorable magnetic properties archeological artifacts are associated with higher success rates in paleointensity experiments. However, their spatial and temporal availability is limited to areas and ages associated with ancient civilizations; the majority of the archeointensity data are derived from Europe [e.g., *Gallet et al*., 2005; *Gómez-Paccard et al*., 2012], the Middle East [e.g., *Ben-Yosef et al*., 2009; *Shaar et al*., 2011; *Ertepinar et al*., 2012], and Mesoamerica [e.g., *Sternberg*, 1989; *Bowles et al*., 2002] and encompasses the last 3–5 millennia. To increase both the resolution and accuracy of geomagnetic field models a better global coverage of high-resolution regional paleointensity curves is indispensible. Therefore, we have to exploit more readily available extrusive igneous rocks with the associated low success rates in paleointensity experiments [*Valet*, 2003]. The magnetic properties of a single cooling unit can vary considerably for different locations in the flow [e.g., *Böhnel et al*., 1997; *Hill and Shaw*, 2000; *Biggin et al*., 2007; *Valet et al*., 2010; *Böhnel et al*., 2011; *de Groot et al*., 2013a]. Variations in chemical and mineralogical composition of the magnetic minerals, their grain size, and cooling rate of the flow all influence the magnetic behavior of the samples during paleointensity experiments.

Recent methodological advances in paleointensity techniques have substantially increased the success rates in obtaining reliable paleointensities from lavas since *Thellier and Thellier* [1959] proposed their paleointensity method in 1959 [e.g., *Coe*, 1967, 1978; *Aitken et al*., 1988; *Hill and Shaw*, 1999; *Riisager and Riisager*, 2001; *Krasa et al*., 2003; *Tauxe and Staudigel*, 2004; *Yu et al*., 2004a; *Yu and Tauxe*, 2005; *Dekkers and Böhnel*, 2006; *Fabian and Leonhardt*, 2010; *Muxworthy*, 2010]. The chance of obtaining a reliable paleointensity estimate for a given cooling unit can be increased from the typical 10–20% up to 60–70% by sampling cooling units

at multiple locations, applying different paleointensity methods to sister specimens, and subjecting the paleointensity results to rigorous quality criteria [*de Groot et al*., 2013b]. A better understanding of the relations between the rock-magnetic properties as a result of volcanic emplacement processes and the chances of obtaining a reliable paleointensity estimate, however, would further increase the success rate and efficiency of paleointensity experiments.

Here we describe the rock-magnetic properties and results of both thermal and pseudo-Thellier experiments as function of depth in a ∼6 m thick lava flow emplaced at ∼588 AD ∼8 km south of Hilo, Hawaii, USA. Samples were taken at different depths in the flow using an elevated work platform; the amount of sample material per depth is therefore limited. Samples from all depths are subjected to extensive rock-magnetic testing, comprising both thermal and alternating field demagnetization experiments, susceptibility-versus-temperature and high-field rock-magnetic analyses before paleointensity experiments were done. Because of the limited amount of sample material multispecimen-style experiments [*Dekkers and Böhnel*, 2006; *Fabian and Leonhardt*, 2010] were not feasible; we choose thermal "IZZI" (in-field, zero-field, zero-field, in-field) Thellier [*Tauxe and Staudigel*, 2004; *Yu et al*., 2004b; *Yu and Tauxe*, 2005] and calibrated pseudo-Thellier [*Tauxe et al*., 1995; *de Groot et al*., 2013b] experiments to assess the magnitude of the paleofield. For the central part of the flow both the thermal and pseudo-Thellier methods yielded interpretable results that are similar for both methods.

Previous studies on variations in rock-magnetic or paleointensity behavior with depth in lava flows dealt with thinner flows (<2 m) [*Hill and Shaw*, 2000; *Vérard et al*., 2012], and reported mostly minor variations in rock-magnetic properties. Earlier studies on thick lavas include work by *Wilson et al*. [1968] and *Ade-Hall et al*. [1968a, 1968b, 1968c] and *Audunssen et al*. [1992] on very thick basaltic flows (up to several tens of meters thick) that were possibly subject to ponding. While these studies report extensive petrography and magnetic property analysis, the paleointensity analysis reported—if performed at all—is rather limited compared to today's standards. Another similar study is by *Böhnel et al*. [2003] who reported paleointensity estimates as a function of depth in a flow with a thickness comparable to the present flow. *Böhnel et al*. [2003] argue that microwave-based paleointensity results are superior to classical thermal Thellier-style results because of multidomain effects combined with alteration at higher temperature. They report a very high success rates for the microwave experiments, much better than earlier Thellier-style work [*Böhnel et al*., 1997]. In the thick lava flow presented here, the rock-magnetic behavior and the suitability of samples for paleointensity experiments appears to vary substantially with depth and can be explained by volcanic emplacement and cooling processes. As we will show most of this flow is, unfortunately, not suited for paleointensity study with a variety of techniques, differing from the *Böhnel et al*. [2003] study that reports high success rates.

2. Geological Setting and Sampling

Holocene lava flows are readily available and accessible on the island of Hawaii (USA); however, thick flows are not often exposed from top to bottom. Here we took samples from a flow that is ∼6 m thick and is exposed in a wall of an abandoned quarry, south of Hilo (19°38.2′N, 155°3.0′W). The flow was radiocarbon dated by *Rubin et al*. [1987], sample number W4981. The obtained laboratory age is 1470 BP ± 50; this laboratory age can be recalibrated with INTCAL.09 [*Reimer et al*., 2009] and Calib 6.0 [*Stuiver and Reimer*, 1993] to a calendar age of 588 AD (1 standard deviation confidence interval: 558–640 AD). This flow is a typical Hawaiian inflated sheet flow, with a lava core that continued to flow while the crust at the top solidified and a basal crust formed at the bottom [*Hon et al*., 1994; *Kauahikaua et al*., 1998]. The cooling rate profile of such a flow is described by *Kattenhorn and Schaefer* [2008]; the top is most efficiently cooled, while some thermal energy dissipates into the underlying flow as well. The slowest cooled part is at approximately two thirds of the flow's thickness from the top; for this flow thus at ∼4 m depth.

The bottom of the flow is at ∼3 m above ground level in the quarry; the samples were taken from the wall using an elevated work platform. The top of the flow was also exposed in a road cut, ∼5 m from the edge of the quarry wall. Groups of 14–19 samples were taken at six different depths in the flow (Figure 1); samples were taken as close together as possible to ensure among-sample homogeneity. These "levels" are labeled with a letter (B–G) and were taken at the following depths from the top of the flow: F at 0.2 m; G at 0.6 m; D at 1.5 m; C at 2.4 m; B at 3.9 m; and E at 5.1 m. In between these levels 10 cores were taken, further

referred to as the "X samples." These latter samples are numbered from bottom to top and were taken at the following depths in the flow: X1 at 5.9 m; X2 at 5.5 m; X3 at 4.7 m; X4 at 4.4 m; X5 at 3.5 m; X6 at 2.9 m; X7 at 2.0 m; X8 at 1.1 m; X9 at 0.8 m; and X10 at 0.6 m. One group of samples was taken from the underlying flow and was labeled "level A"; the age of this underlying flow is unknown.

The outcrop seems homogenous from top to bottom, and the drilled cores do also not vary visually in color or mineral content. A thin section was made for each level in the flow (supporting information Figure S1). The phenocrysts, mostly equant large olivine crystals (up to a few millimeters in diameter) are identified by their typical appearance and high refraction index and birefringence. Occasionally, zoning is observed near their rims. Phenocrysts seem to occur in similar amounts and are of similar size regardless the position in the flow. Calcium-rich plagioclase and clinopyroxene can be identified as well. They are notably smaller in size than the olivine, but distinctly larger than the groundmass. As with the olivine, plagioclase and pyroxene seem to be similar in size independent of position within the flow. The grain size in the groundmass, however, differs with depth in the flow: for the top (F, G, and D) and bottom (E) levels the groundmass is finer grained than for the central levels (B and C). Those latter levels reveal a slightly, but visible, coarser groundmass. The thin sections were further subjected to a scanning electron microscopy (SEM) study using a JCM-6000 table top SEM (back scatter images, acceleration voltage 15 kV) (Figure 2). For each sample level, an overview SEM photograph is provided as well as a picture of a typical titanomagnetite at a large magnification. The titanomagnetites show up as the brighter particles. Their oxidation class varies between I and III according to *Haggerty* [1976]. At level F, intergrown aggregates have sizes of ~50 μm, occasionally up to 100 μm (Figure 2a). Individual particles are smaller; a larger grain is shown in Figure 2b (oxidation class I). Very small grains are present but only in small amounts. Level G has aggregates of similar size (Figure 2c) while smaller individual particles (e.g., Figure 2d, oxidation class I) are more prevalent than at level F. Very small particles occur more often. In level D, the intergrown aggregates seem to be largely absent which results in smaller titanomagnetites (Figures 2e and 2f). A distinctly finer set of particles is

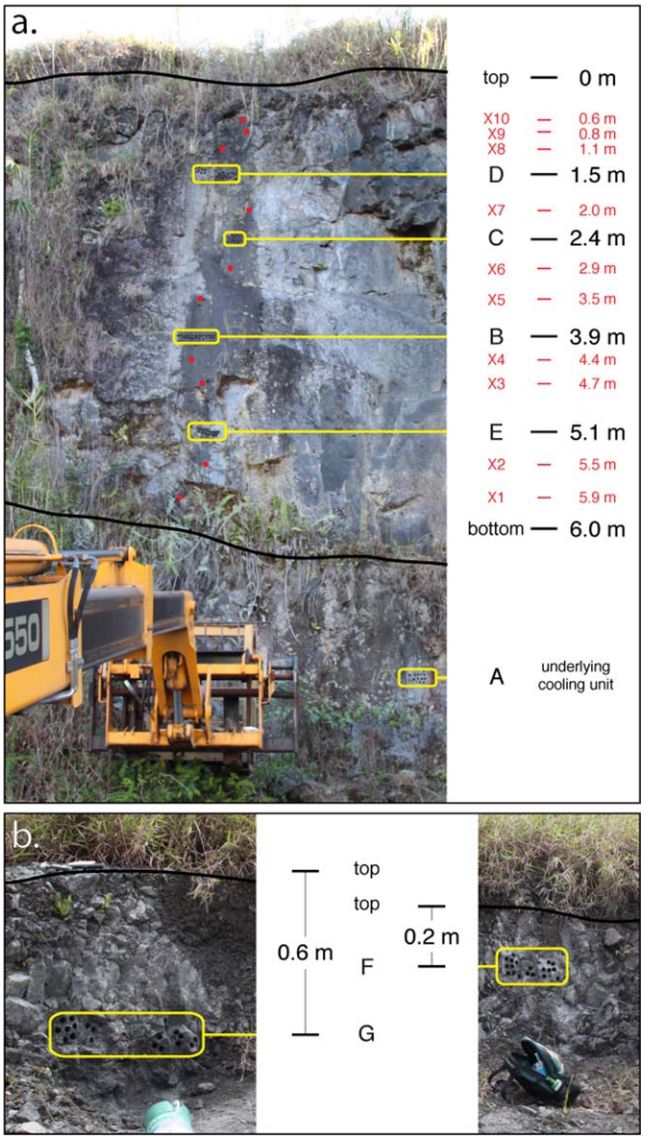

Figure 1. Sampling of the vertical profile. Black lines indicate top and bottom of the flow. Groups of samples ("levels") were taken at 0.2, 0.6, 1.5, 2.4, 3.9, and 5.1 m from the top of the flow, indicated by yellow boxes. Note that the levels, labeled with letters B–G, are not labeled in order. Ten additional cores ("X samples") were taken at different depths in the flow, (a) labeled from bottom to top, indicated by the red dots. Levels F and G were taken from a outcrop on top of the lava flow, (b) <5 m away from the vertical profile. One group of samples was taken from the underlying flow: "level A."

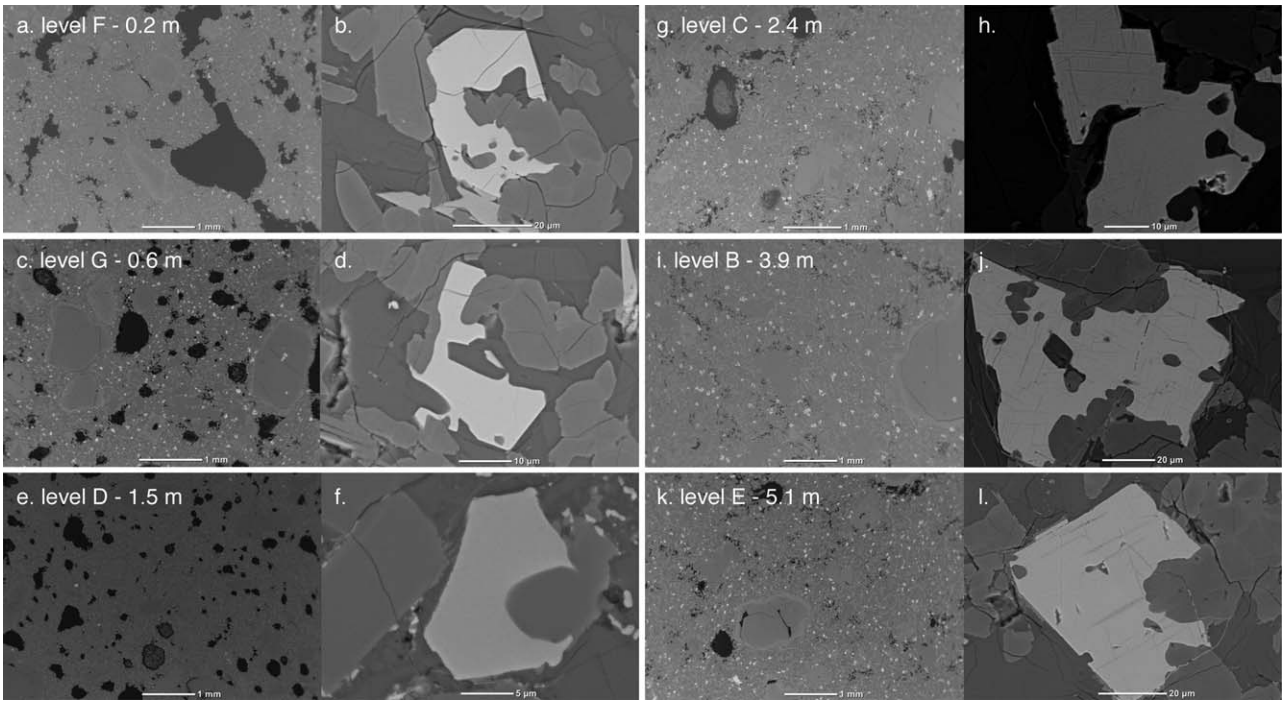

Figure 2. Scanning electron microscope (SEM) images of all levels. For each level, an overview image is on the left and a detailed image of a titanomagnetite grain is on the right. Note (h and j) the lamellae visible in the titanomagnetite grains in levels C and B and (b and d) the lack of such lamellae in titanomagnetites at levels F and G. Titanomagnetites at levels D and E have less and less distinct lamellae.

present as well (Figure 2f, oxidation class I–II). Exsolution structures occur only occasionally in contrast to deeper parts of the flow. Levels C and B are characterized by larger intergrown aggregates of up to 100 μm in size next to finer particles (Figures 2g and 2i). At level B, short chains of these particles occur (Figure 2i) while they seem to be less prominent at level C (Figure 2g). Noteworthy is that the titanomagnetites are exsolved ubiquitously at these two levels (Figures 2h and 2j, oxidation class III) indicating slower cooling. The deepest level E has rather small aggregates of titanomagnetites, ∼50 μm in size (Figure 2k), slightly smaller aggregates than levels C and B, in line with its faster cooling. Some exsolution lamellae are observed (Figure 2l, oxidation class II) but they occur in much smaller amounts and are finer in structure than at levels C and B.

In the topmost levels F and G exsolution structures were not observed, but submicroscopic lamellae of course cannot be excluded. This implies that the top two levels, F and G, and to some degree also D and the lowermost level E, cooled faster than the central levels (B–C). This is typical for an inflated lava flow where a liquid core continues to flow underneath a solidified crust. In the topmost levels F and G two suites of titanomagnetite grains seem to be present: rather coarse-grained often irregular shaped grains are accompanied by numerous smaller grains.

Optically opaques are equant and intimately intergrown with randomly oriented aggregates of fine laths of plagioclase and pyroxene. Their concentration in the groundmass is estimated to be ∼5% (difficult to gauge for level D for which the thin section has a larger thickness), phenocrysts are essentially devoid of opaques. In level E there are less opaques visible, which would concur with a lower specific saturation magnetization for this level.

3. Methods

Samples from the six levels (B–G) were subjected to a number of rock-magnetic analyses and pseudo-Thellier paleointensity experiments. The limited amount of sample material of the X samples only permitted bulk susceptibility and high-field rock-magnetic analyses for these levels.

3.1. Demagnetization Experiments

The NRM of at least 10 samples per level was stepwise demagnetized using either alternating fields (AF) or thermal steps. The samples were AF demagnetized with a robotized 2G DC-SQUID magnetometer to less than 10% of their NRM in 15 steps: 2.5, 5, 7.5, 10, 15, 20, 25, 30, 40, 50, 60, 70, 80, 90, and 100 mT. Two samples per level were subjected to thermal demagnetization using a 2G DC-SQUID magnetometer and an ASC TD-48SC thermal demagnetizer. The thermal steps for levels E, F, and G were 110, 160, 210, 270, 340, 410, 500, and 580°C; for levels B, C, and D the temperatures were set at: 110, 160, 260, 350, 420, 480, 530, and 580°C. The NRM was generally demagnetized to less than 3% at 580°C.

3.2. Susceptibility

The bulk susceptibility of at least 10 samples per level and all X samples was measured on an AGICO KLY-3 susceptometer. Furthermore, the susceptibility of the six levels was assessed as function of temperature on the same AGICO KLY-3 susceptometer with CS3 furnace attachment. The temperature was increased in cycles to test for irreversibility of the signal. Peak temperatures were set at ~225, 330, 430, 500, 560, and 600°C. To test for thermochemical alteration the temperature was lowered at least 50°C after reaching each peak temperature; alteration is indicated by an irreversible cooling temperature segment. Thermochemical alteration in the samples hampers a reliable thermal paleointensity experiment; temperatures higher than the "alteration temperature"—defined here as the highest peak temperature that shows reversible behavior—cannot be safely utilized in thermal paleointensity experiments.

Furthermore, the Curie temperature can be inferred from the susceptibility-versus-temperature (χ-T) diagrams as the inflection point after a peak in susceptibility. Magnetite (Fe_3O_4) has a distinct Curie temperature indicated by a sharp drop in susceptibility at 550–580°C; if Fe is substituted with Ti to form titanomagnetites ($Fe_{3-x}Ti_xO_4$ with $0 \leq x \leq 1$) the Curie temperature is lowered [*Dunlop and Özdemir*, 1997]. Other potentially substituting elements such as Al and Mg are also known to further lower the Curie temperature of titanomagnetites [*Richards et al*., 1973].

3.3. High-Field Rock-Magnetic Analyses

The saturation magnetization (M_s), remanent saturation magnetization (M_{rs}), coercive force (B_c), and remanent coercive force (B_{cr}) were measured on a Princeton instruments alternating gradient force magnetometer, PMC Model 2900. Specimens are generally between 5 and 10 mg; at least three chips were measured for each level and all X samples. The saturating field was set to 1 T; to correct for the paramagnetic contribution, the linear high-field segment of the loops was subtracted. Complete saturation of the ferromagnetic contribution is assumed at 800 mT, well within the linear segment. Heterogeneities in the bulk material caused rather substantial variations among chips from the same level; therefore, the same four parameters were measured on a Quantum Design physical property measurement system (PPMS) in combination with a vibrating sample magnetometer (VSM) measurement system (saturating field 1.5 T), which is capable of measuring samples with a much larger mass of typically 1 g. The ratios M_{rs}/M_s and B_{cr}/B_c indicate the grain-size distribution of the magnetic carriers [*Day et al*., 1977; *Dunlop*, 2002]. Hawaiian lavas are typically within the pseudo-single-domain grain size range (M_{rs}/M_s between 0.05 and 0.5; B_{cr}/B_c between 1.5 and 4). The grain size influences the behavior of samples during paleointensity experiments: single domain (SD) grains ($M_{rs}/M_s > 0.5$ and $B_{cr}/B_c < 1.5$) behave ideally; PSD and multidomain (MD; $M_{rs}/M_s < 0.05$ and $B_{cr}/B_c > 4$) are associated with nonideal behavior that may hamper paleointensity experiments.

3.4. First-Order Reversal Curves

First-order reversal curves (FORCs) [*Pike et al*., 1999; *Roberts et al*., 2000] were obtained for all levels with the same Princeton instruments alternating gradient force magnetometer as used for the hysteresis loop measurements. The saturating field was also set to 1 T; field increment to ~2 mT; 200 FORC curves were obtained. The curves were processed with the FORCinel2 package [*Harrison and Feinberg*, 2008] with the VARIFORC addition [*Egli*, 2013]; smoothing factors were set at 3, and both lambdas at 0.1. This enables extrapolation to $B_c = 0$ region with minimal distortion because of incomplete FORC grids and offers higher resolution in the regions of the FORC diagrams where most change in FORC density occurs. The potential effects of SP particles with their FORC density close to the ordinate axis [*Pike et al*., 2001a] can thus be evaluated.

Table 1. IZZI-Thellier Results[a]

Sample	int.	st. dev.	sel. crit.	T	n	f	g	q	α	β	MAD Free	Drat	CK-Error
PICRIT-03			P		$\geq$4	$\geq$0.35		$\geq$0.2	$<$15	$\leq$0.1	$<$7	$\leq$7	
SELCRIT-1			S		$\geq$4	$\geq$0.15		$\geq$1	$<$15	$\leq$0.1	$<$15	$\leq$10	
CLASS-A			A		$\geq$7	$\geq$0.70		$\geq$5	$<$10	$\leq$0.1	$<$7	$\leq$12.5	
B1	39.9	2.1	P, S, A	300–580	7	0.94	0.76	13.7	0.8	0.05	2.6	2.4	3.2
B2	37.9	1.3	P, S, A	20–580	8	0.97	0.75	20.9	0.9	0.03	2.5	2.8	4.0
C1	52.0	3.8	P, S, A	20–580	8	0.97	0.68	9.1	0.8	0.07	6.2	1.6	2.5
C2	45.6	4.1	P, S, A	20–580	8	0.98	0.69	7.6	0.8	0.09	4.0	3.5	5.7
D1	32.7	2.3	P, S	300–540	6	0.61	0.58	5.1	1.1	0.07	6.0	6.0	4.7
D1*	48.2	3.6	S	20–500	6	0.58	0.61	4.8	5.4	0.07	7.7	6.6	6.0
$n = 5$	*41.6*	*7.4* *18%*											

[a]For all samples that pass at least one of the sets of selection criteria used in this study as specified on the top three rows the following parameters are given: sample name; obtained paleointensity (int.); standard deviation associated with this intensity (st. dev.); selection criteria passed (P = PICRIT-03 [*Kissel and Laj*, 2004], S = SELCRIT-1 [*Selkin and Tauxe*, 2000; *Biggin et al*., 2007], A = CLASS-A) (sel. crit.); temperature segment interpreted (T); number of points included in the linear regression (n); fraction (f), gap (g), and quality (q) parameters [*Coe*, 1978]; angle between the floating and origin-anchored linear fits through the Zijderveld diagrams (α); ratio of the standard error of the linear fit to the slope (β); maximum angular deviation (MAD free); and the maximum difference ratio for the pTRM-checks (DRAT) [*Selkin and Tauxe*, 2000]. Sample D1* refers to the alternative interpretation of the Aria diagram of this particular sample (the gray dashed line in Figure 7a). The average paleointensity based on the accepted IZZI-Thellier results is on bottom row, together with its 1 standard deviation.

3.5. IZZI-Thellier Experiments

In Thellier-style paleointensity experiments—the classical technique to obtain absolute estimates of the paleointensity for samples that acquired their remanent magnetization by cooling in the Earth's paleofield—the NRM of the samples is progressively replaced by imparted pTRMs in a known magnetic field. The magnitude of the paleofield is reconstructed by comparing the remaining NRM and the induced pTRM for the same temperature steps. Since its introduction in 1959 [*Thellier and Thellier*, 1959], several refinements and improvements have been proposed, mainly to reduce the adverse effects of nonideal grain sizes in samples [e.g., *Coe*, 1967, 1978; *Aitken et al*., 1988; *McClelland and Briden*, 1996; *Selkin and Tauxe*, 2000; *Riisager and Riisager*, 2001; *Tauxe and Staudigel*, 2004; *Yu et al*., 2004b].

Two samples per level (a total of 12 samples) are subjected to the "IZZI" (In-field, Zero-field, Zero-field, In-field) protocol [*Tauxe and Staudigel*, 2004; *Yu et al*., 2004b; *Yu and Tauxe*, 2005], in which the in-field and zero-field steps alternate. The temperature steps used in the IZZI-Thellier experiments were adjusted based on the thermal demagnetization behavior of sister specimens. Samples from the top of the flow (levels F and G) unblock a large part of their NRM for relatively low temperatures: for these levels, the following temperature steps were used: 60, 90, 120, 150, 180, 210, 240, 270, 300, 330, and 360°C. Both pTRM-checks [*Prévot et al*., 1985] and tail-checks [*McClelland and Briden*, 1996] were done at 60, 120, 180, 240, and 300°C. For the other levels, the steps used were: 100, 150, 200, 250, 300, 350, 400, 450, 500, 540, and 580°C, with pTRM-checks and tail-checks at 100, 200, 300, 400, 500, and 580°C. Samples from levels B, C, and D skipped the temperature steps until 300°C to avoid unnecessary heating of the samples, because they unblock less than 10% at this temperature in the thermal demagnetization experiments.

To interpret the IZZI-Thellier results, we used the program ThellierTool 4.2 by *Leonhardt et al*. [2004]. To assess the technical quality of our IZZI-Thellier results, we calculated a number of Thellier-parameters: n, the number of data interpreted for the linear fit; f, the fraction of the NRM used for the linear fit [*Coe*, 1978]; g, the gap factor [*Coe*, 1978]; q, the quality factor [*Coe*, 1978]; α, the angle between the floating and origin-anchored linear fits through the Zijderveld diagrams; β, the ratio of the standard error of the linear fit to the slope; free-floating MAD, the maximum angular deviation; and DRAT, the maximum difference ratio for the pTRM-checks [*Selkin and Tauxe*, 2000]. Based on these parameters each IZZI-Thellier result was assessed using three sets of selection criteria: SELCRIT-1 [*Selkin and Tauxe*, 2000; *Biggin et al*., 2007], PICRIT-03 [*Kissel and Laj*, 2004], and "CLASS-A." The latter was defined to focus on the number of data points ($N \geq 7$) and NRM fraction ($f \geq 0.7$) to be used for the linear fit in the Arai plot to exclude sagging. CLASS-A is marginally less strict for the DRAT parameter than PICRIT-03 and SELCRIT-1, but stricter for the other parameters included (Table 1).

3.6. Pseudo-Thellier Experiments

The thermal steps needed to impart the pTRMs in IZZI-Thellier experiments are known to potentially induce both chemical and magnetic alteration [e.g., *Valet*, 2003; *Tauxe and Staudigel*, 2004; *Biggin et al*., 2007;

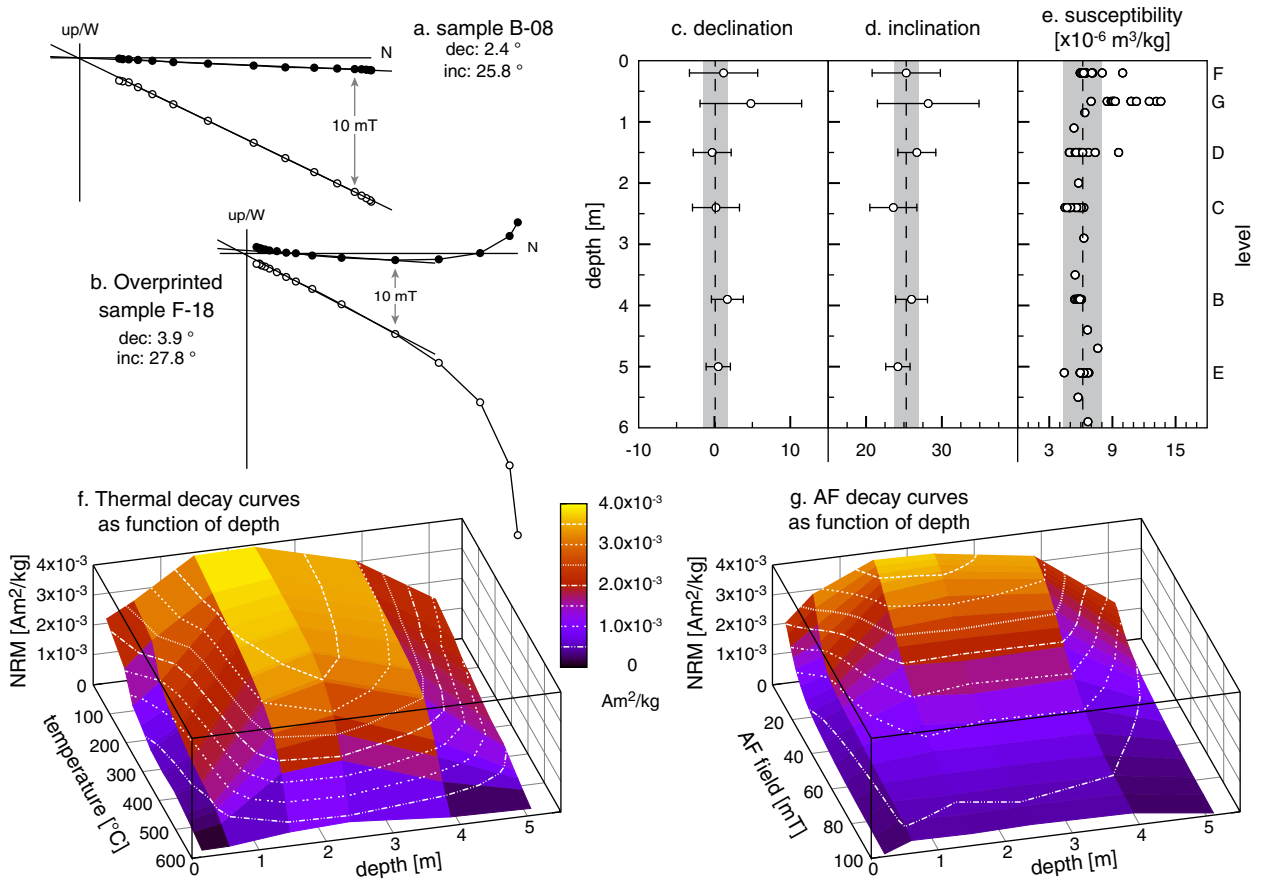

Figure 3. Demagnetization behavior of the natural remanent magnetization. All samples from levels B, C, and D, and most samples from levels E, F, and G, have univectorial demagnetization behavior toward the origin in a Zijderveld diagram (example in Figure 3a). Some samples from sites E, F, and G, however, have overprints that are readily removed at 10 mT (example in Figure 3b). (c and d) The declination and inclination of the characteristic remanent magnetization are constant throughout the lava flow for all levels (levels are indicated on the right); the average declination and inclination are depicted by a dashed line, together with its α_{95} (shaded area). Both the (f) thermal and (g) AF decay curves differ with increasing depth in the flow. The NRM is given on the vertical axis, the depth in the flow from left to right, and the temperature or the peak AF on the axis from back to front; colors are proportional to the NRM; NRM isolines (5×10^{-4} Am^2/kg intervals) are in white (dashed in various styles). The specific NRM is almost twice as high between 1.5 and 4 m from the top of the flow, compared to the top (F) and bottom (E) levels. Furthermore, the NRM of the samples is unblocked at higher temperatures or alternating fields for the central part of the flow. (e)The bulk susceptibility of the samples is constant below 0.8 m from the top; the average susceptibility is depicted by a dashed line, together with its 1 standard deviation confidence interval (shaded area).

de Groot et al., 2013a]. Sedimentary rocks are not suitable for these absolute paleointensity experiments, since they did not acquire their remanent magnetization by cooling in the Earth's magnetic field. To obtain relative paleointensity information from sedimentary stratigraphies *Tauxe et al.* [1995] proposed the pseudo-Thellier method. In the pseudo-Thellier method magnetizations in the samples are not removed and imparted thermally, but by using alternating fields. Since the samples are not heated potential chemical and magnetic alteration are therefore avoided. *Yu et al.* [2003] explored its potential on lavas and found that the outcome of pseudo-Thellier experiments depends on the grain-size distribution in the samples. To apply the pseudo-Thellier technique to lavas on a large scale, a grain-size selector is therefore needed. *de Groot et al.* [2013b] proposed $B_{1/2ARM}$, the AF field required to impart half of the saturation ARM in the samples. Utilizing a densely sampled historical field record on Hawaii, they obtained an empirically calibrated formula to convert pseudo-Thellier results that pass the proposed selection criterion to absolute paleointensities. Samples with a $B_{1/2ARM}$ between 23 and 63 mT can be converted to absolute paleointensities using the empirical formula: B_{abs} (μT) = 7.371 * |pseudo-Thellier slope| + 14.661 (under the premise that the DC-field applied during the ARM-acquisitions is set to 40 μT).

Here we subject six samples per level to a pseudo-Thellier experiment. First, the NRM of the samples is stepwise AF demagnetized at the following peak fields: 2.5, 5, 7.5, 10, 15, 20, 25, 30, 40, 50, 60, 70, 80, 90, 100,

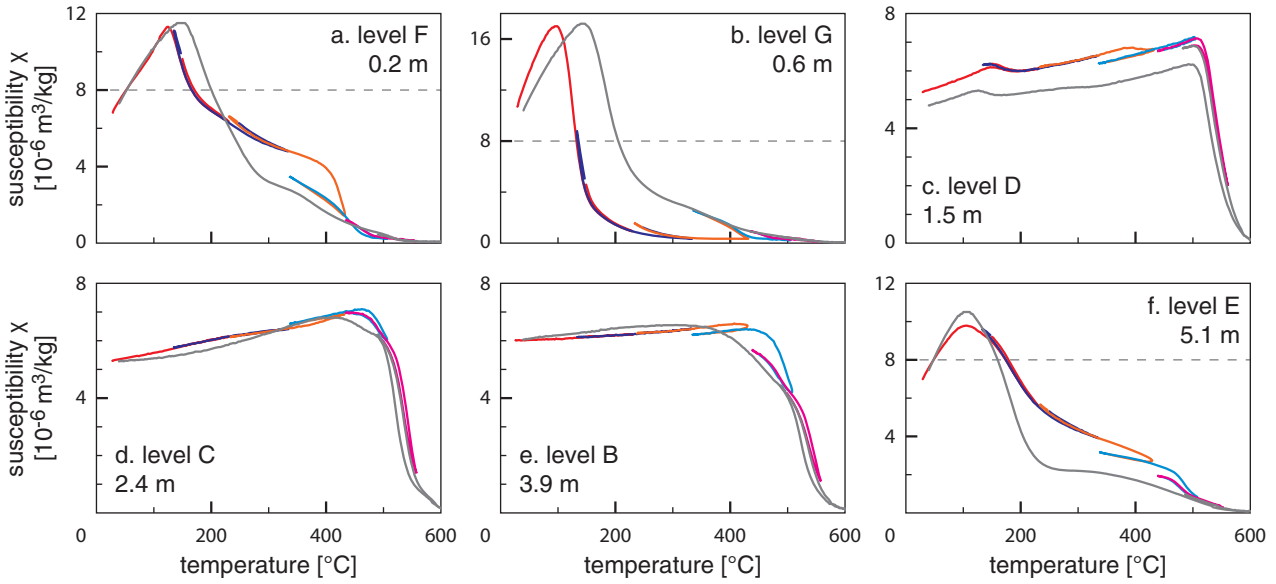

Figure 4. Susceptibility behavior as function of temperature and depth in the flow. The six thermal cycles all have their own color. Note that the scale on the vertical axis is not the same for all plots: the maximum susceptibility value in Figures 4c–4e (8.0×10^{-6} m^3/kg) is indicated by a dashed line in the other plots. The thermal behavior of the susceptibility varies as function of depth: the behavior in the central part of the flow mostly resembles that of magnetite (TM-0), while the behavior toward the top and bottom reveal a higher Ti-content (up to TM-65). Alteration does not occur before reaching 330°C, (d) for level C, the entire cycle up to 600°C is reversible.

150, 225, and 300 mT. The NRM is demagnetized to less than 3% at 300 mT. AF coils attached to the robotized system apply field steps up to 100 mT, higher field steps are applied in a laboratory-built AF coil. Second, ARMs are imparted on the same samples at the same field steps using a DC bias field of 40 μT on the robotized magnetometer setup. The ARM acquisition curves appear to reach full saturation above 150 mT. The last step is to demagnetize the saturated ARM in the samples, again using the same field steps. All measurements are done on the robotized 2G DC-SQUID magnetometer. Since anisotropy is generally low in lavas (below 2%) the NRM and ARMs can be reliably compared, even if their orientation in the samples is not the same.

To obtain reliable pseudo-Thellier slopes, the same grains that carried the NRM must acquire the ARM during the pseudo-Thellier experiment. To evaluate the segment of AF fields that should be interpreted in the Arai plot, first the ARM demagnetization is plotted against the NRM demagnetization behavior. If the NRM and ARM are carried by the same grains, a linear trend toward the origin would be expected from this diagram. The Arai plots (NRM remaining-versus-ARM gained) are therefore only interpreted for the AF steps for which the ARM demagnetization-versus-NRM demagnetization diagram shows linear behavior toward the origin.

4. Results

4.1. Demagnetization Experiments

Both the magnitude of the NRM and its demagnetization behavior varies with depth in the flow (Figures 3f and 3g). For the central part of the flow (levels D and C at 1.5 and 2.4 m), the specific NRM is $\sim 3.8 \times 10^{-3}$ Am^2/kg; just below the top of the flow (level F at 0.2 m), the specific NRM is $\sim 2.1 \times 10^{-3}$ Am^2/kg. At the bottom of the flow (level E at 5.1 m), the specific NRM is only $\sim 1.4 \times 10^{-3}$ Am^2/kg. Levels B and G have intermediate specific NRMs. In both the thermal and AF demagnetization experiments, the top and bottom levels (E, F, and G) are demagnetized at lower temperatures or alternating fields than the levels in the central part of the flow (levels B, C, and D). The top and bottom levels are demagnetized to ~50% of their NRM at 10 mT, while the central levels retain 50% of their NRM at 30–35 mT. Thermal demagnetization indicates that the top and bottom levels lose 50% of their NRM at ~200°C, while the samples from the central part of the flow retain more than 50% of their NRM at ~500°C.

All samples from levels B, C, and E have univectorial demagnetization behavior toward the origin of the Zijderveld diagrams (Figure 3a). Some samples from levels E, F, and G, have minor (viscous) overprints before

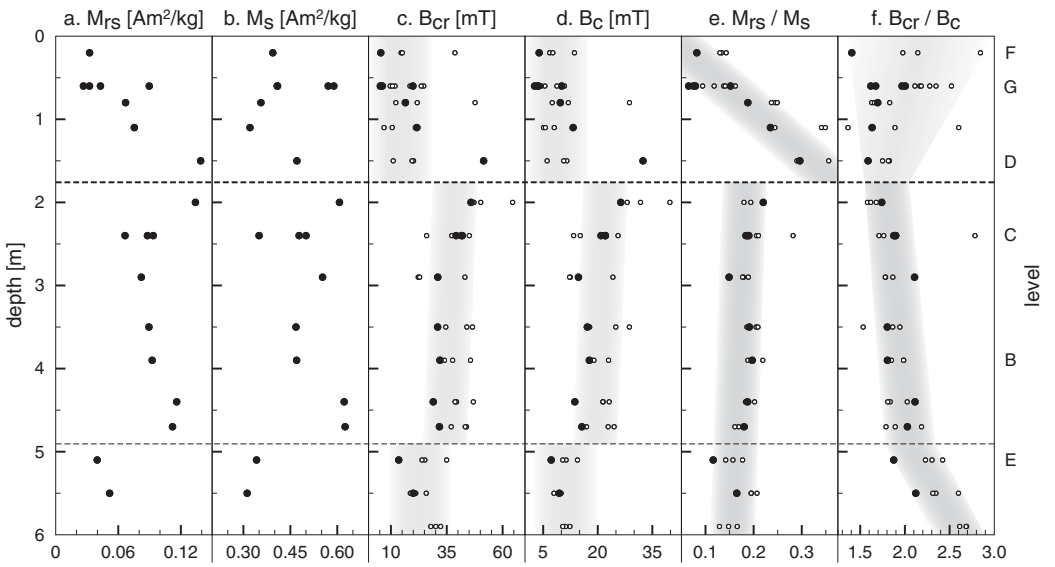

Figure 5. High-field rock-magnetic analyses. In all plots, data acquired using a VSM (sample size typically ~1 g) are solid black dots; data acquired using an AGM (sample size typically ~5 mg) are open dots. Trends with depth in the flow are tentatively shaded. In the (a) M_{rs} and (b) M_s plots the AGM data are omitted, because the mass of the samples is too low to obtain a reliable representation of the bulk lava per mass. The (c) B_{cr} and (d) B_c values are generally lower for the top and bottom parts of the flow. (e) The M_{rs}/M_s ratio reveals the most distinctive trends with depth: in the top part of the flow the M_{rs}/M_s ratio varies from ~0.08 at 0.2 m from the top to ~0.30 at 1.5 m. Further downward, the M_{rs}/M_s ratio decays from ~0.20 at 2 m from the top to ~0.15 at 0.1 m from the bottom. The levels in the flow are indicated on the right-hand side of the figure, dashed lines tentatively indicate the top, central, and bottom parts of the flow based on changes in trends in the depicted parameters.

demagnetizing toward the origin. These are generally removed at 10 mT; 10 mT, however, demagnetizes ~50% of these samples' NRM (Figure 3b). The obtained declinations and inclinations are the same for all levels to within the α_{95} confidence interval (Figures 3c and 3d), as expected since the entire flow cooled in several months at most. Note that the between-specimen variation is higher in the quicker cooled topmost levels G and F. The mean declination and inclination for all samples from this flow are 0.1 and 25.3°, respectively, with a α_{95} confidence interval of 1.6° (shaded in Figures 3c and 3d). This substantiates that all levels in the upper flow cooled within months and therefore are one single cooling unit. The declination and inclination of the underlying flow (level A in Figure 1) are 6.4 and 32.0°, with a α_{95} of 5.9°. These directions differ significantly from the directions in the overlying flow. The underlying flow containing level A must therefore be substantially older.

4.2. Susceptibility

The bulk susceptibility at room temperature appears to be constant, independent of position in the flow: 6.29×10^{-6} m^3/kg with a standard deviation of 1.72×10^{-6} m^3/kg (Figure 3e). Level G (0.6 m from the top) is an exception: it reveals a distinctly higher susceptibility: 1.02×10^{-5} m^3/kg. Furthermore, the variation in susceptibility between samples is higher for the top part of the flow.

The behavior of the susceptibility as function of temperature reveals varying behavior for the top and bottom levels (E, F, and G), and the levels in the central part of the flow (B, C, and D) (Figure 4). Levels D and C (1.5 and 2.4 m from the top) have a dominant high Curie temperature at ~550°C, while the Curie temperature of level B (3.9 m from the top) is somewhat lower at ~490°C. Level G (0.6 m from the top) has the lowest Curie temperature in the profile: ~120°C. Level F (0.2 m from top) has two distinct Curie temperatures at ~160°C and ~430°C, although the latter may be influenced by thermochemical alteration. The same applies to level E (5.1 m from top) with the lower Curie temperature at ~200°C and the higher at ~490°C, but definitely influenced by alteration as evidenced by an irreversible cooling path. The susceptibility is reversible through temperature cycles up to 330°C for all samples; level C at 2.4 m from the top does not show any signs of alteration even after heating to 600°C (Figure 4d). The observed χ-T behavior is in line with the demagnetization behavior. The top and bottom levels are demagnetized at lower temperatures corresponding with lower Curie temperatures in the χ-T diagrams.

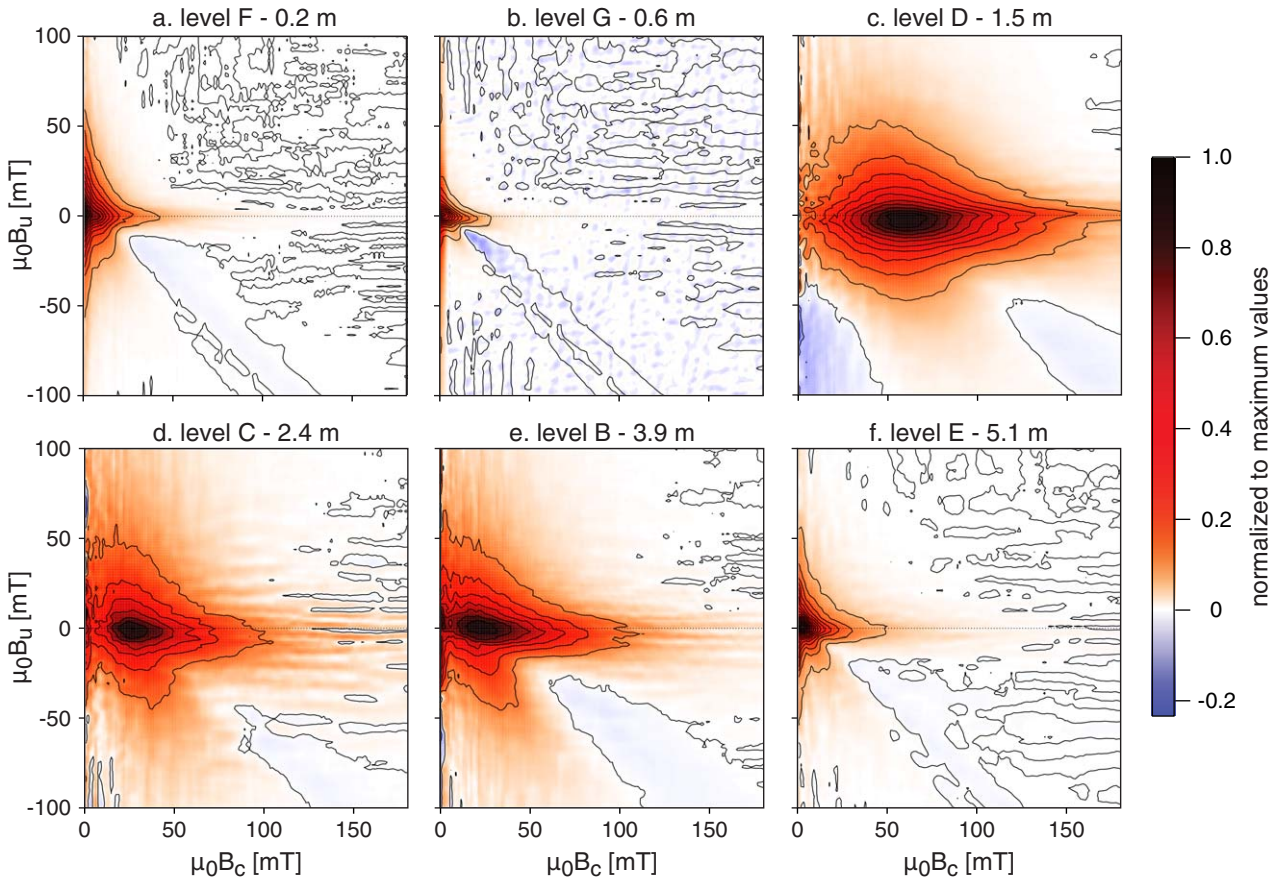

Figure 6. First-order reversal curves as a function of depth in the flow. In all diagrams, the smoothing factor is 3. Each diagram is scaled to its maximum value. The color coding is indicated on the right; all data are normalized to their maximum occurring value. See also main text.

4.3. High-Field Rock-Magnetic Analyses

The high field rock-magnetic parameters M_{rs}, M_s, B_{cr}, and B_c and their ratios show distinct trends with depth in the flow (Figure 5). B_{cr} and B_c are generally lower for the top (top to 1.5 m depth) and bottom (from 5.1 m to bottom) parts of the flow. The average B_{cr} for the top is ~12 mT, for the central part of the flow ~39 mT, and for the bottom part ~25 mT. B_c varies from ~9.5 mT at the top, to ~21.5 mT for the central part, and ~10 mT for the bottom part of the flow. A tentative trend in the central part of the flow is indicated for both B_{cr} and B_c: at 2 m below the top the B_{cr} and B_c values seem slightly higher than at 4.7 m from the top.

The B_{cr}/B_c ratio suggests a trend from top to bottom through the entire flow: the ratio increases with increasing depth—although the scatter in this ratio is large, especially in the top part of the flow. The trends in the M_{rs}/M_s ratio are better constrained. In the top part of the flow, the M_{rs}/M_s ratio increases linearly from ~0.08 at 0.2 m from the top to ~0.30 at 1.5 m. Furthermore, the M_{rs}/M_s ratio seems to decrease though the central and bottom parts of the flow from ~0.20 at 2 m from the top to ~0.15 at 0.1 m from the bottom. Hysteresis loops and a Day plot [*Day et al.*, 1977; *Dunlop*, 2002] are included in supporting information Figure S2.

4.4. First-Order Reversal Curves

In FORC diagrams, magnetically interacting ensembles of SD particles are characterized by concentric contours centered on the FORC density maximum at B_c ($\mu_0 H_c$). Noninteracting SD particles have their FORC density concentrated close to and centered on the $B_u = 0$ axis [e.g., *Egli et al.*, 2010]. MD particles have vertical contours centered on the B_c density maximum [*Pike et al.*, 2001b]. The topmost two levels, F and G, are characterized by a fair amount of SP particles (Figure 6). Also the lowermost level E has a conspicuous fine-grained particle contribution. Along the $B_u = 0$ axis is the "high-field" tail of the SP contribution straddling

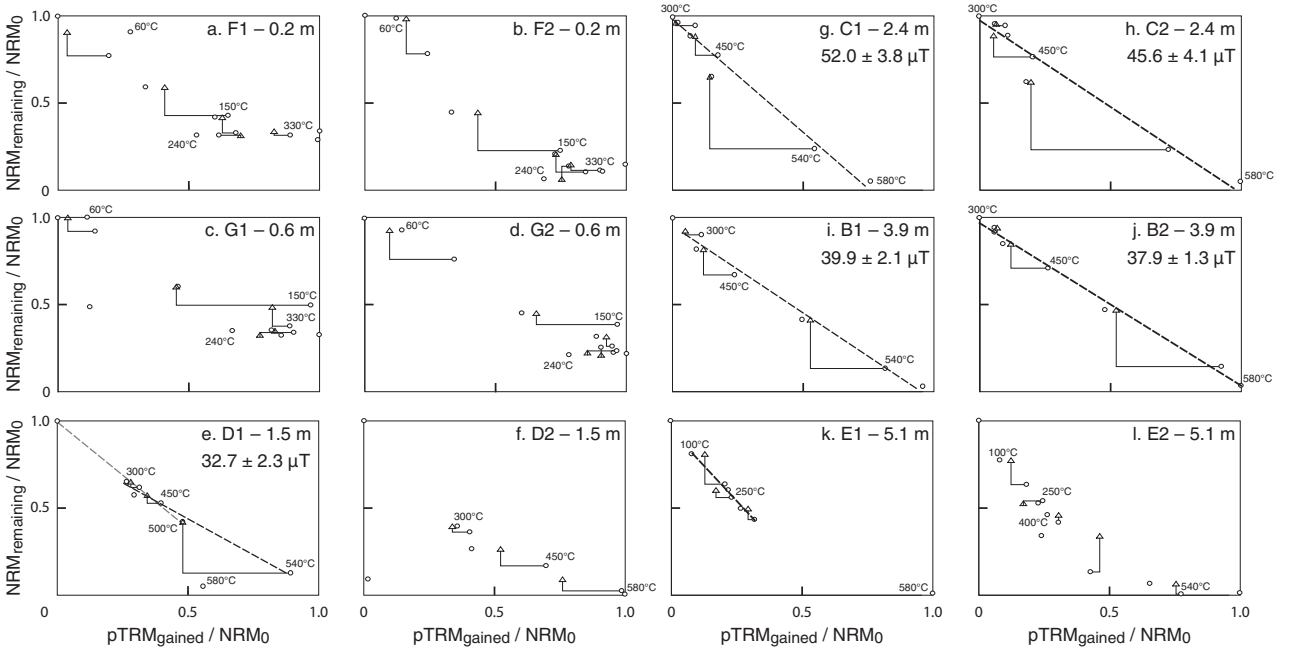

Figure 7. IZZI-Thellier results. All obtained results are shown (two samples per level); only five yielded interpretable results, i.e., passed at least one set of selection criteria (see main text). Both the NRM remaining (vertical axis) and the pTRM gained (horizontal axis) are normalized to the full NRM (NRM_0) of the sample. Data are depicted as open circles; checks are open triangles; and the interpreted linear regression is shown as a dashed black line. The level (expanded by sample number 1 or 2), depth below the top of the flow and—if applicable—the obtained paleointensity (together with its standard error) are given in the top-right corner of each plot. Some temperatures are indicated at certain data points. The gray dashed line in Figure 7e is the alternative interpretation of sample D1 and corresponds to "D1*" in Table 1 (see main text).

into the PSD realm. Truly MD particles would have more vertical contour lines. Please note that some samples from levels F and G show considerable directional overprints (Figure 3b). Levels F and E show more magnetic interaction than level G. Level D exhibits closed FORC contours typical of magnetically interacting SD particles with a remarkably small contribution of SP particles. The coercivity FORC density maximum is at ~65 mT, high for nominally SD titanomagnetite, which hints at possible exsolution features beyond the resolution of the SEM. The coercivity FORC density maximum lowers to ~20–30 mT in levels C and B, where the SEM images revealed ubiquitous exsolution structures. The FORC diagrams resemble those of PSD particles with their triangular contours intersecting at $B_c = 0$ [*Muxworthy and Dunlop*, 2002] combined with a portion of SP particles as evidenced by increased FORC density very close to the ordinate axis of the respective diagrams. At fields slightly higher than those of the SP contribution the FORC contours have a tendency to close (they become narrower spaced around the $B_u = 0$ axis). The triangular contour lines typical of PSD particles are not yet fully developed, which presumably indicates a dominant particle size range at the lower (SD) end of the PSD realm. Note that the exsolution structures result in a magnetic grain size smaller than the optical grain size. Because of the close spacing of the intergrowths magnetic interaction is clearly present.

4.5. IZZI-Thellier Results

The IZZI-Thellier results for levels B and C (the central part of the flow) were technically successful: all of their samples pass all three sets of selection criteria (Figure 7 and Table 1). The samples from level B yield 39.9 ± 2.1 and 37.9 ± 1.3 μT; the samples from level C 52.0 ± 3.8 and 45.6 ± 4.1 μT. The Arai diagrams of the sister samples from each level are remarkably similar. One sample from level D passes both the PICRIT-03 and SELCRIT-1 criteria if interpreted between 300 and 540°C, which yields 32.7 ± 2.3 μT (black dashed line in Figure 7a, line "D1" in Table 1); however, this sample also passes the SELCRIT-1 criteria if interpreted between 20 and 500°C and yields 48.2 ± 3.6 μT (the gray dashed line in Figure 7a, line "D1*" in Table 1). Since this latter estimate fails the PICRIT-03 criteria, we adhere to the interpretation between 300 and 540°C for this sample. The other sample from level D and the samples from levels E, F, and G (the top and bottom of the flow) are technically unsuccessful. The average paleointensity obtained using the IZZI-Thellier

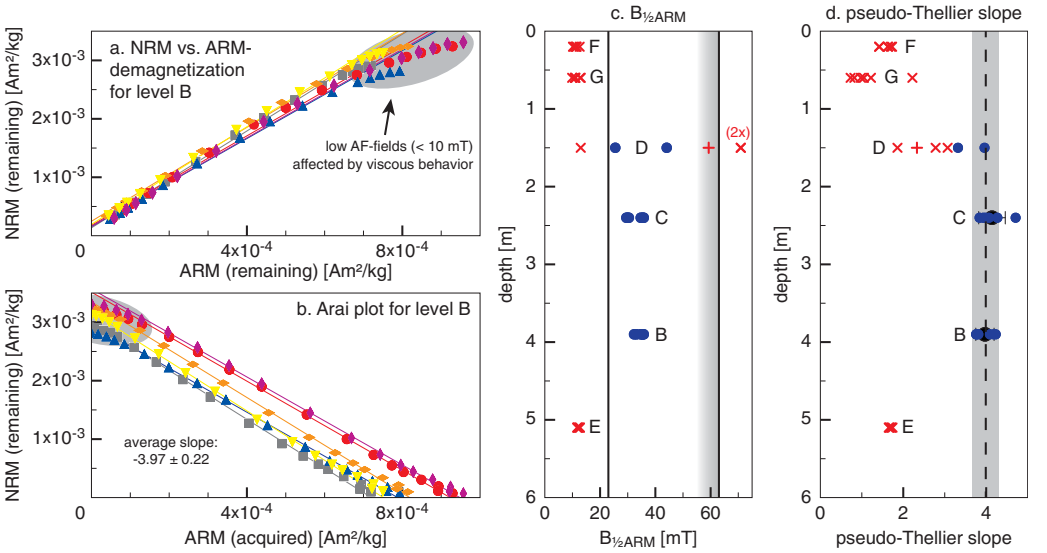

Figure 8. Pseudo-Thellier results. (a and b) The six samples in the NRM-versus-ARM demagnetization diagram and the Arai plot for level B are depicted with each their own symbol and color (Arai diagrams for the other levels are in the supporting information). The nonlinear behavior for low AF steps is indicated with gray shading. (b)The average slope for the six samples from level B is indicated in the bottom-left corner of the Arai diagram. (c and d) The obtained $B_{1/2ARM}$'s and pseudo-Thellier slopes are remarkably similar within each level, except for level D. Samples from level D have notably variable behavior in the pseudo-Thellier experiments; one sample from that particular level reveals sagging behavior in its Arai diagram and is therefore omitted from further analyses (the red "+" in Figures 8c and 8d), see supporting information figure. (c) The boundaries of the $B_{1/2ARM}$ window are solid lines, the shading on the upper boundary denoting some uncertainty is the same shading as in *de Groot et al.* [2013a, 2013b]. Samples not passing the $B_{1/2ARM}$ selection criterion are depicted as red crosses, samples passing this criterion as blue dots. For levels C and D, an average pseudo-Thellier slope could be calculated together with is 1 standard deviation confidence interval, depicted as solid black dots with horizontal error bars. (d) The average pseudo-Thellier slope for all samples from the vertical profile that pass the selection criterion is indicated as a dashed line, together with its 1 standard deviation confidence interval (shaded area).

protocol for this flow is based on five samples passing the selection criteria used: 41.6 ± 7.4 μT, with the standard deviation being 18% of the paleointensity estimate.

4.6. Pseudo-Thellier

Within all levels—except level D—the variations in behavior among the samples is remarkably small for both $B_{1/2ARM}$ and the pseudo-Thellier slope (Figure 8). Most samples exhibit linear behavior in the NRM-versus-ARM demagnetization and Arai diagrams for alternating fields higher than 10 mT, the nonlinear behavior for field steps below 10 mT is attributed to viscous behavior of the samples. The pseudo-Thellier slopes are therefore generally calculated using the AF steps between 10 and 100 mT. Details of all processed samples and all Arai plots are provided in supporting information Table S1 and Figure S3, respectively.

All samples from levels E, F, and G, the top and bottom levels have $B_{1/2ARM}$'s below 23 mT (Figure 8c) in line with the FORC density maxima at comparatively low values. They do therefore not pass the selection criterion as proposed by *de Groot et al.* [2013b]. The $B_{1/2ARM}$'s of samples from levels B and C range between 25 and 40 mT. Samples from level D show a remarkable spreading in $B_{1/2ARM}$'s ranging from 13.0 to 70.9 mT, with three samples passing the selection criterion. One of these samples however, shows distinct "sagging" in its Arai diagram with an inflection point at 40–50 mT, it is therefore excluded from further analyses (the red "+" in Figures 8c and 8d).

The value of the pseudo-Thellier slope for all samples that do not pass the $B_{1/2ARM}$ selection criterion is lower than for samples that do pass this criterion (Figure 8d). This applies to samples with a $B_{1/2ARM} < 23$ mT and those with $B_{1/2ARM} > 63$ mT. The pseudo-Thellier slopes for the samples that do pass the $B_{1/2ARM}$ criterion are remarkably constant for all levels: the average absolute slope for the entire flow is 3.99 with a standard deviation of 0.32. With the empirical calibration formula of *de Groot et al.* [2013b], this pseudo-Thellier slope corresponds to an absolute paleointensity of 44.1 ± 2.4 μT.

5. Discussion

5.1. Rock-Magnetic Variations

At ~1.5 m below the top the flow, most rock-magnetic parameters change suddenly. The Curie temperature and unblocking temperature spectra increase by ~300°C; the FORC diagrams reveal a distinctly different grain-size distribution and the trends in the high-field rock-magnetic parameters change. These observations are best explained by the transition from the crust of the inflated sheet flow to what was the originally liquid lava core. The top 1.5 m cooled quickly—in hours to days—while the lava core continued to flow, for weeks up to possibly several months before solidifying. The base of the lava flow, where the lava solidified to form the basal crust of an inflated sheet flow [*Hon et al*., 1994; *Kauahikaua et al*., 1998], has magnetic properties similar to those in the top.

5.2. Titanium Content in Remanence Carrying Grains

Thermal demagnetization of the NRM and χ-T experiments are mutually supportive indicating lower unblocking temperature spectra and Curie temperatures for the top and bottom parts of the flow, and higher unblocking temperature spectra and Curie temperatures for the central part of the flow. The titanium content in the titanomagnetite solid solution is deterministic for both the Curie and unblocking temperatures: the magnetite end-member (TM0, Fe_3O_4) has a Curie and maximum unblocking temperature of ~580°C, while the magnetic ordering temperature for ulvöspinel (TM100, Fe_2TiO_4), the other end-member, is −153°C, i.e., far below room temperature [*Dunlop and Özdemir*, 1997]. According to their Curie temperatures, the titanium content in the titanomagnetite varies from TM65 at the top of the flow, to TM0 in the central part, and TM55 at the bottom [*Lattard et al*., 2006]. It is important to note, however, that the titanium composition of the bulk lava is expected to be approximately constant from top to bottom as it is a single cooling unit erupted from a single magma chamber.

The variations in titanium content observed from the rock-magnetic experiments concur with the SEM observations. The titanomagnetites in the slow cooling parts—at levels B and C and to a lesser extend in levels D and E—revealed distinct exsolution structures, i.e., lamellae, while such features are not visible in the faster cooling parts. Apparently the longer time at relatively higher temperatures allows a better unmixing of the titanomagnetites to exsolve into the compositions of the two end-members of the magnetite-ulvöspinel solid solution. In the slow cooling parts of the lava, the titanomagnetites unmixes into the magnetite end-member with high Curie and blocking temperatures that carries the magnetic remanence. In the parts of the flow that cooled much faster, the bottom and especially the top part of the flow, the titanomagnetites are (variably) quenched (without visible exsolution structures) to form titanomagnetites with intermediate composition, with the associated intermediate Curie and blocking temperatures.

5.3. Physical Versus Magnetic Grain Sizes

The Bcr/Bc ratios obtained by the high-field rock-magnetic analyses are relatively low in the central part of the flow and somewhat higher in the faster cooled, upper and bottom parts. Generally, this could be interpreted as the grains being smaller in the slower cooled parts and larger toward the top and bottom parts. This is counterintuitive to the cooling rate profile: a slower cooling gives more time for crystal-growth and therefore larger grains. An explanation may be found in the occurrence of exsolution lamellae in the central part of the flow; they may act as dividers in the grain that pin domain walls similar to imperfections in the crystal lattice [*Schmidt*, 1973; *Xu and Merrill*, 1989, 1990]. We hypothesize that magnetic grains may therefore behave magnetically "smaller" (i.e., more SD-like) than expected by their actual physical size.

5.4. Consequences for Paleointensity Methods

It is argued that titanomagnetites that unblock the majority of their magnetic remanence within a narrow range of the Curie temperatures are better suitable for (thermal) paleointensity experiments [*Valet et al*., 2010]. Samples with low Curie and unblocking temperatures are more vulnerable to viscous overprints, since less thermal energy is needed to unblock their magnetization; viscous overprints potentially hamper a reliable paleointensity experiment. Therefore, often samples with a low Ti-content (hence a high Curie temperature) are often regarded as suitable material for paleointensity experiments; however, high temperatures must be reached during the experiments on such samples, increasing the risk of chemical and magnetic alteration. In Thellier-style experiments, the temperature steps for which the NRM is affected by a viscous overprint cannot be interpreted, but a reliable paleointensity estimate might still be obtained using

the higher temperature steps. Multispecimen (MSP)-style experiments [*Dekkers and Böhnel*, 2006; *Fabian and Leonhardt*, 2010] demand the samples to be aligned with their natural TRM in the direction of the applied DC field in the furnace; this is impossible for samples with a viscous overprint and the MSP-style paleointensity experiments are therefore not possible for these samples. Samples with low Curie temperatures and unblocking temperatures must be tested rigorously for overprints before they can be subjected to MSP-style paleointensity results. Furthermore, both samples with high and low Curie temperatures must therefore be rigorously tested for the occurrence of magnetic alteration at temperatures used in paleointensity experiments [*de Groot et al*., 2012].

Our IZZI-Thellier experiments are technically successful for the slower cooled parts of the flow where the magnetic remanence is carried by relatively Ti-poor titanomagnetites and narrow ranges of Curie temperatures; this is in line with the findings of *Valet et al*. [2010]. It is unlikely that our samples suffer from either chemical or magnetic alteration at higher temperatures during the experiments, since the pTRM-checks return to the corresponding data points within reasonable error. For the faster cooled parts of the flow, however, the IZZI-Thellier experiments fail and are not interpretable. This implies that samples with higher Ti-content suffer more from either chemical alteration (e.g., progressive unmixing) or magnetic alteration (e.g., trans-domain changes) than Ti-poor titanomagnetites. We hypothesize that the occurrence of lamellae and the associated "smaller" magnetic behavior may also have a positive effect on the chances of obtaining a reliable paleointensity estimate.

Here we showed that the cooling rate has a major influence on the rock-magnetic properties and therefore the samples' suitability for paleointensity experiments. The chance of obtaining a reliable estimate for a single cooling unit without any prior knowledge of the unit's rock-magnetic properties can therefore be increased considerably by sampling at various depths in the flow and test the reversibility and stability of rock-magnetic behavior of the samples before commencing any paleointensity experiments.

5.5. Pseudo-Thellier Selection Criteria

The application of the pseudo-Thellier method [*Tauxe et al*., 1995] to lavas depends on a proper grain-size selector. Only samples with similar grain size and therefore comparable coercive behavior can be faithfully utilized [*Yu et al*., 2003]. *de Groot et al*. [2013b] proposed to use the alternating field value that imparts half of the saturated ARM, $B_{1/2ARM}$, as grain size selector; this parameter can directly be obtained from pseudo-Thellier experiments. Samples with a $B_{1/2ARM}$ between 23 and 63 mT—a rather wide range—yielded proper results and can be converted into absolute paleointensity estimates following a linear relation [*de Groot et al*., 2013b].

The linear relation that was proposed to convert pseudo-Thellier results in absolute estimates of the paleointensity is based on a significant number of samples; however, they all were taken in one volcanic edifice and all acquired their NRM in ambient fields between 35 and 40 μT. The proposed regression does not go through the origin; therefore, the applicability outside the interval used for calibration must be further assessed. It must be noted, however, that the pseudo-Thellier results outside this interval do agree well with results obtained using other, more established, paleointensity techniques [*de Groot et al*., 2013b]. The pseudo-Thellier results obtained in this study yielded absolute paleointensity estimates between 40 and 50 μT—just above the range of field intensities on which the calibration relation is based. Our results can therefore be used faithfully—certainly to compare them with the obtained thermal Thellier results and the outcome of other rock-magnetic experiments.

It maybe argued that the selection criterion for pseudo-Thellier results as proposed by *de Groot et al*. [2013b] accepts samples with a rather wide range of coercive behavior. All samples in this study that pass the selection criterion, however, yielded similar pseudo-Thellier results—independent of variations in rock-magnetic parameters other than $B_{1/2ARM}$. It must be noted that the $B_{1/2ARM}$ values of all samples that pass in this data set are between 23 and 50 mT, the only sample with a higher $B_{1/2ARM}$, below 63 mT, D-2, showed sagging behavior in its Arai plot (see supporting information Figure S3) and was therefore excluded from further analyses. Since the upper limit of the $B_{1/2ARM}$ window for samples that yield reliable results was also not very well constrained by the data of *de Groot et al*. [2013b], the empirical upper limit of 63 mT may be subject to further debate. Nevertheless, the pseudo-Thellier method with the proposed selection criterion yielded robust results—largely independent of the rock-magnetic properties of the samples other than $B_{1/2ARM}$.

The calibrated pseudo-Thellier method as proposed by *de Groot et al.* [2013b] seems to have great potential as an addition to existing paleointensity techniques, although it is evident that much work still needs to be done to assess the full potential of this method. With a better understanding of the relation between grain size, titanium content, $B_{1/2ARM}$ and pseudo-Thellier result, the selection criterion for the pseudo-Thellier method and the calibration to absolute paleointensities may be further enhanced.

5.6. IZZI-Thellier Versus Pseudo-Thellier Results

The obtained calibrated pseudo-Thellier paleointensity for the entire flow (44.1 $\pm$ 2.4 μT) is in good agreement with the thermal Thellier result (41.6 $\pm$ 7.4 μT) and other paleointensity results for approximately this age in the intensity record of *de Groot et al.* [2013b]. A Wilcoxon rank-sum test for the accepted IZZI-Thellier data ($n = 5$) and the accepted pseudo-Thellier data ($n = 16$) yields a two-tailed p value of 0.78. Therefore, the results of the experiments are indistinguishable at the 5% significance level ($p \geq 0.05$).

It is remarkable that the thermal Thellier results seem to trend slightly with depth in the flow: from 32.7 μT at 2.4 m below the top (level D) to 48.8 μT at 2.4 m below the top (level C), to 38.9 μT at 3.9 m below the top (level B). This tentative trend is hard to explain: we cannot exclude that the paleointensities recorded at different depths in the flow were affected by local anomalies at the time of cooling. It is also possible that the rock-magnetic properties of the samples lead to slight overestimates or underestimates of the "true" (and unknown) paleofield during paleointensity experiments. The results of the pseudo-Thellier experiments are also relatively low at 1.5 m below the top (41.5 μT). The pseudo-Thellier results of levels B and C, however, are indistinguishable; their averages are, respectively, 45.2 and 43.9 μT. If the same trend is present in the pseudo-Thellier results, it is less pronounced than the trend in the thermal Thellier results.

6. Conclusions

Rock-magnetic parameters that govern the behavior of samples during paleointensity experiments vary as function of depth in a lava flow. These variations can be explained by the amount of titanomagnetite exsolution that is accommodated by the cooling rate during emplacement of the lava flow. The suitability of samples for paleointensity experiments depends on their rock-magnetic properties. The chance of obtaining a reliable paleointensity can therefore be increased by sampling lavas at multiple levels at different distances from the top of the flow and careful preliminary testing of the rock-magnetic properties. The calibrated pseudo-Thellier results that pass the selection criterion proposed by *de Groot et al.* [2013b] yield an average paleointensity of 44.1 $\pm$ 2.4 μT. This is in good agreement with the paleointensity obtained by thermal Thellier experiments (41.6 $\pm$ 7.4 μT) and the record proposed by *de Groot et al.* [2013b].

Acknowledgments

We gratefully acknowledge Ken Hon for his suggestions and help during our fieldwork. The people at Business Services Hawaii are acknowledged for granting access to their premises and for the use of their cherry picker to take the samples. Greig Paterson and Harald Böhnel are gratefully acknowledged for their thorough and constructive reviews that greatly helped to improve this manuscript. This research was funded by a grant from the Earth and Life Science Division (ALW) of the Netherlands Organization for Scientific Research (NWO); the robotized magnetometer was acquired with a grant of the equipment fund of NWO.

References

Ade-Hall, J.-M., M. A. Khan, P. Dagley, and R. L. Wilson (1968a), A detailed opaque petrological and magnetic investigation of a single Tertiary lava flow from Skye, Scotland-I. Iron-titanium oxide petrology, *Geophys. J. R. Astron. Soc.*, *16*, 375–388.

Ade-Hall, J.-M., M. A. Khan, P. Dagley, and R. L. Wilson (1968b), A detailed opaque petrological and magnetic investigation of a single Tertiary lava flow from Skye, Scotland-II. Spatial variations of magnetic properties and selected relationships between magnetic and opaque petrological properties, *Geophys. J. R. Astron. Soc.*, *16*, 389–399.

Ade-Hall, J.-M., M. A. Khan, P. Dagley, and R. L. Wilson (1968c), A detailed opaque petrological and magnetic investigation of a single Tertiary lava flow from Skye, Scotland-III. Investigations into the possibility of obtaining the intensity of the ambient magnetic field (F_{ANC}) at the time of the cooling of the flow, *Geophys. J. R. Astron. Soc.*, *16*, 401–415.

Aitken, M., A. Allsop, G. Bussell, and M. Winter (1988), Determination of the intensity of the Earth's magnetic field during archaeological times: Reliability of the Thellier technique, *Rev. Geophys.*, *26*(1), 3–12.

Audunssen, H., S. Levi, and F. Hodges (1992), Magnetic property zonation in a thick lava flow, *J. Geophys. Res.*, *97*(B4), 4349–4360.

Ben-Yosef, E., L. Tauxe, T. E. Levy, R. Shaar, H. Ron, and M. Najjar (2009), Geomagnetic intensity spike recorded in high resolution slag deposit in Southern Jordan, *Earth Planet. Sci. Lett.*, *287*(3–4), 529–539, doi:10.1016/j.epsl.2009.09.001.

Biggin, A. J., M. Perrin, and M. J. Dekkers (2007), A reliable absolute palaeointensity determination obtained from a non-ideal recorder, *Earth Planet. Sci. Lett.*, *257*(3–4), 545–563, doi:10.1016/j.epsl.2007.03.017.

Böhnel, H., J. Morales, C. Caballero, L. Alva, G. McIntosh, S. Gonzalez, and G. J. Sherwood (1997), Variation of rock magnetic parameters and paleointensities over a single Holocene lava flow, *J. Geomagn. Geoelectr.*, *49*(4), 523–542.

Böhnel, H., A. J. Biggin, D. Walton, J. Shaw, and J. A. Share (2003), Microwave palaeointensities from a recent Mexican lava flow, baked sediments and reheated pottery, *Earth Planet. Sci. Lett.*, *214*, 221–236.

Böhnel, H., E. Herrero-Bervera, and M. J. Dekkers (2011), *Paleointensities of the Hawaii 1955 and 1960 Lava Flows: Further Validation of the Multi-specimen Method*, pp. 195–211, Springer, Dordrecht, Netherlands.

Bowles, J., J. Gee, J. Hildebrand, and L. Tauxe (2002), Archaeomagnetic intensity results from California and Ecuador: Evaluation of regional data, *Earth Planet. Sci. Lett.*, *203*(3–4), 967–981.

Coe, R. (1978), Geomagnetic paleointensities from radiocarbon-dated lava flows on Hawaii and the question of the Pacific nondipole low, *J. Geophys. Res.*, *83*(B4), 1740–1756.
Coe, R. S. (1967), Paleo-intensities of the Earth's magnetic field determined from Tertiary and Quaternary rocks, *J. Geophys. Res.*, *72*(12), 3247–3262.
Day, R., M. Fuller, and V. Schmidt (1977), Hysteresis properties of titanomagnetites: Grain-size and compositional dependence, *Phys. Earth Planet. Inter.*, *13*, 260–267.
de Groot, L. V., M. J. Dekkers, and T. A. T. Mullender (2012), Exploring the potential of acquisition curves of the anhysteretic remanent magnetization as a tool to detect subtle magnetic alteration induced by heating, *Phys. Earth Planet. Inter.*, *194–195*, 71–84, doi:10.1016/j.pepi.2012.01.006.
de Groot, L. V., T. A. T. Mullender, and M. J. Dekkers (2013a), An evaluation of the influence of the experimental cooling rate along with other thermomagnetic effects to explain anomalously low palaeointensities obtained for historic lavas of Mt Etna (Italy), *Geophys. J. Int.*, *193*(3), 1198–1215, doi:10.1093/gji/ggt065.
de Groot, L. V., A. J. Biggin, M. J. Dekkers, C. G. Langereis, and E. Herrero-Bervera (2013b), Rapid regional perturbations to the recent global geomagnetic decay revealed by a new Hawaiian record, *Nat. Commun.*, *4*, 1–7, doi:10.1038/ncomms3727.
Dekkers, M. J., and H. N. Böhnel (2006), Reliable absolute palaeointensities independent of magnetic domain state, *Earth Planet. Sci. Lett.*, *248*(1–2), 508–517, doi:10.1016/j.epsl.2006.05.040.
Dunlop, D. J. (2002), Theory and application of the Day plot (Mrs/Ms versus Hcr/Hc) 1. Theoretical curves and tests using titanomagnetite data, *J. Geophys. Res.*, *107*(B3), 2056, doi:10.1029/2001JB000486.
Dunlop, D. J., and Ö. Özdemir (1997), *Cambridge Studies in Magnetism: Rock Magnetism: Fundamentals and Frontiers*, pp. 1–1, Cambridge Univ. Press, Cambridge, U. K.
Egli, R. (2013), VARIFORC: An optimized protocol for calculating non-regular first-order reversal curve (FORC) diagrams, *Global Planet. Change*, *110*, 302–320, doi:10.1016/j.gloplacha.2013.08.003.
Egli, R., A. P. Chen, M. Winklhofer, K. P. Kodama, and C.-S. Horng (2010), Detection of noninteracting single domain particles using first-order reversal curve diagrams, *Geochem. Geophys. Geosyst.*, *11*, Q01Z11, doi:10.1029/2009GC002916.
Ertepinar, P., C. G. Langereis, A. J. Biggin, M. Frangipane, T. Matney, T. Ökse, and A. Engin (2012), Archaeomagnetic study of five mounds from Upper Mesopotamia between 2500 and 700 BCE Further evidence for an extremely strong geomagnetic field ca. 3000 years ago, *Earth Planet. Sci. Lett.*, *357–358*, 84–98, doi:10.1016/j.epsl.2012.08.039.
Fabian, K., and R. Leonhardt (2010), Multiple-specimen absolute paleointensity determination: An optimal protocol including pTRM normalization, domain-state correction, and alteration test, *Earth Planet. Sci. Lett.*, *297*(1–2), 84–94, doi:10.1016/j.epsl.2010.06.006.
Gallet, Y., A. Genevey, and F. Fluteau (2005), Does Earth's magnetic field secular variation control centennial climate change?, *Earth Planet. Sci. Lett.*, *236*(1–2), 339–347, doi:10.1016/j.epsl.2005.04.045.
Gómez-Paccard, M., et al. (2012), Improving our knowledge of rapid geomagnetic field intensity changes observed in Europe between 200 and 1400 AD, *Earth Planet. Sci. Lett.*, *355–356*, 131–143, doi:10.1016/j.epsl.2012.08.037.
Haggerty, S. E. (1976), Opaque mineral oxides in terrestrial igneous rocks, in *Oxide Minerals, Short Course Notes*, vol. 3: Hg101–Hg300, edited by D. H. Rumble, III, Mineral. Soc. of Am. Short Course Notes.
Harrison, R. J., and J. M. Feinberg (2008), FORCinel: An improved algorithm for calculating first-order reversal curve distributions using locally weighted regression smoothing, *Geochem. Geophys. Geosyst.*, *9*, Q05016, doi:10.1029/2008GC001987.
Hill, M. J., and J. Shaw (1999), Palaeointensity results for historic lavas from Mt Etna using microwave demagnetization/remagnetization in a modified Thellier-type experiment, *Geophys. J. Int.*, *139*(2), 583–590.
Hill, M. J., and J. Shaw (2000), Magnetic field intensity study of the 1960 Kilauea lava flow, Hawaii, using the microwave palaeointensity technique, *Geophys. J. Int.*, *142*, 487–504.
Hon, K., J. Kauahikaua, R. Denlinger, and K. Mackay (1994), Emplacement and inflation of pahoehoe sheet flows: Observations and measurements of active lava flows on Kilauea Volcano, Hawaii, *Geol. Soc. Am. Bull.*, *106*(3), 351–370, doi:10.1130/0016-7606(1994)106<0351:EAIOPS>2.3.CO;2.
Kattenhorn, S. A., and C. J. Schaefer (2008), Thermal–mechanical modeling of cooling history and fracture development in inflationary basalt lava flows, *J. Volcanol. Geotherm. Res.*, *170*(3–4), 181–197, doi:10.1016/j.jvolgeores.2007.10.002.
Kauahikaua, J., K. V. Cashman, T. N. Mattox, C. C. Heliker, K. A. Hon, M. T. Mangan, and C. R. Thornber (1998), Observations on basaltic lava streams in tubes from Kilauea Volcano, island of Hawai'i, *J. Geophys. Res.*, *103*(B11), 27,303–27,323.
Kissel, C., and C. Laj (2004), Improvements in procedure and paleointensity selection criteria (PICRIT-03) for Thellier and Thellier determinations: Application to Hawaiian basaltic long cores, *Phys. Earth Planet. Inter.*, *147*(2–3), 155–169, doi:10.1016/j.pepi.2004.06.010.
Krasa, D., C. Heunemann, R. Leonhardt, and N. Petersen (2003), Experimental procedure to detect multidomain remanence during Thellier-Thellier experiments, *Phys. Chem. Earth*, *28*, 681–687.
Lattard, D., R. Engelmann, A. Kontny, and U. Sauerzapf (2006), Curie temperatures of synthetic titanomagnetites in the Fe-Ti-O system: Effects of composition, crystal chemistry, and thermomagnetic methods, *J. Geophys. Res.*, *111*, B12S28, doi:10.1029/2006JB004591.
Leonhardt, R., C. Heunemann, and D. Krasa (2004), Analyzing absolute paleointensity determinations: Acceptance criteria and the software ThellierTool4.0, *Geochem. Geophys. Geosyst.*, *5*, Q12016, doi:10.1029/2004GC000807.
McClelland, E., and J. C. Briden (1996), An improved methodology for Thellier-type paleointensity determination in igneous rocks and its usefulness for verifying primary thermoremanence, *J. Geophys. Res.*, *101*(B10), 21,995–22,013.
Muxworthy, A. R. (2010), Revisiting a domain-state independent method of palaeointensity determination, *Phys. Earth Planet. Inter.*, *179*(1–2), 21–31, doi:10.1016/j.pepi.2010.01.003.
Muxworthy, A. R., and D. J. Dunlop (2002), First-order reversal curve (FORC) diagrams for pseudo-single-domain magnetites at high temperature, *Earth Planet. Sci. Lett.*, *203*(1), 369–382.
Pike, C. R., A. P. Roberts, and K. L. Verosub (1999), Characterizing interactions in fine magnetic particle systems using first order reversal curves, *J. Appl. Phys.*, *85*(9), 6660–6667.
Pike, C. R., A. P. Roberts, and K. L. Verosub (2001a), First-order reversal curve diagrams and thermal relaxation effects in magnetic particles, *Geophys. J. R. Astron. Soc.*, *145*(3), 721–730.
Pike, C. R., A. P. Roberts, M. J. Dekkers, and K. L. Verosub (2001b), An investigation of multi-domain hysteresis mechanisms using FORC diagrams, *Phys. Earth Planet. Inter.*, *126*(1), 11–25.
Prévot, M., E. A. Mankinen, R. S. Coe, and C. S. Gromme (1985), The Steens Mountain (Oregon) geomagnetic polarity transition 2. Field intensity variations and discussion of reversal models, *J. Geophys. Res.*, *90*(B12), 10,417–10,448.
Reimer, P. J., et al. (2009), IntCal09 and Marine09 radiocarbon age calibration curves, 0–50,000 years cal BP, *Radiocarbon*, *51*(4), 1111–1150.

Richards, J., J. B. O'Donovan, Z. Hauptman, W. O'Reilly, and K. M. Creer (1973), A magnetic study of titanomagnetite substituted by magnesium and aluminium, *Phys. Earth Planet. Inter.*, *7*(4), 437–444.
Riisager, P., and J. Riisager (2001), Detecting multidomain magnetic grains in Thellier palaeointensity experiments, *Phys. Earth Planet. Inter.*, *125*, 111–117.
Roberts, A. P., C. R. Pike, and K. L. Verosub (2000), First-order reversal curve diagrams: A new tool for characterizing the magnetic properties of natural samples, *J. Geophys. Res.*, *105*(28), 461–428.
Rubin, M., L. Kelley-Gargulinski, and J. P. McGeehin (1987), Hawaiian radiocarbon dates, *U.S. Geol. Surv. Prof. Pap.*, *1350*(1), 213–242.
Schmidt, V. A. (1973), A multidomain model of thermoremanence, *Earth Planet. Sci. Lett.*, *20*, 440–446.
Selkin, P. A., and L. Tauxe (2000), Long-term variations in palaeointensity, *Philos. Trans. R. Soc. A*, *358*(1768), 1065–1088.
Shaar, R., E. Ben-Yosef, H. Ron, L. Tauxe, A. Agnon, and R. Kessel (2011), Geomagnetic field intensity: How high can it get? How fast can it change? Constraints from Iron Age copper slag, *Earth Planet. Sci. Lett.*, *301*(1–2), 297–306, doi:10.1016/j.epsl.2010.11.013.
Sternberg, R. S. (1989), Archaeomagnetic paleointensity in the American Southwest during the past 2000 years, *Phys. Earth Planet. Inter.*, *56*(1), 1–17.
Stuiver, M., and P. J. Reimer (1993), Extended 14C data base and revised CALIB 3.0 14C age calibration program, *Radiocarbon*, *35*, 215–230.
Tauxe, L., and H. Staudigel (2004), Strength of the geomagnetic field in the Cretaceous Normal Superchron: New data from submarine basaltic glass of the Troodos Ophiolite, *Geochem. Geophys. Geosyst.*, *5*, Q02H06, doi:10.1029/2003GC000635.
Tauxe, L., T. Pick, and Y. Kok (1995), Relative paleointensity in sediments: A pseudo-Thellier approach, *Geophys. Res. Lett.*, *22*(21), 2885–2888.
Thellier, E., and O. Thellier (1959), Sur l'intensité du champ magnétique terrestre dans le passé historique et géologique, *Ann. Geophys.*, *15*, 285–376.
Valet, J. (2003), Time variations in geomagnetic intensity, *Rev. Geophys.*, *41*(1), 1004, doi:10.1029/2001RG000104.
Valet, J.-P., E. Herrero-Bervera, J. Carlut, and D. Kondopoulou (2010), A selective procedure for absolute paleointensity in lava flows, *Geophys. Res. Lett.*, *37*, L16308, doi:10.1029/2010GL044100.
Vérard, C., R. Leonhardt, and M. Winklhofer (2012), Variations of magnetic properties in thin lava flow profiles: Implications for the recording of the Laschamp Excursion, *Phys. Earth Planet. Inter.*, *200–201*, 10–27, doi:10.1016/j.pepi.2012.03.012.
Wilson, R. L., S. E. Haggerty, and N. D. Watkins (1968), Variation of palaeomagnetic stability and other parameters in a vertical traverse of a single Icelandic lava, *Geophys. J. R. Astron. Soc.*, *16*, 79–96.
Xu, S., and R. T. Merrill (1989), Microstress and microcoercivity in multidomain grains, *J. Geophys. Res.*, *94*(B8), 10,627–10,636.
Xu, S., and R. T. Merrill (1990), Microcoercivity, bulk coercivity and saturation remanence in multidomain materials, *J. Geophys. Res.*, *95*(B5), 7083–7090.
Yu, Y., and L. Tauxe (2005), Testing the IZZI protocol of geomagnetic field intensity determination, *Geochem. Geophys. Geosyst.*, *6*, Q05H17, doi:10.1029/2004GC000840.
Yu, Y., D. J. Dunlop, and Ö. Özdemir (2003), Are ARM and TRM analogs? Thellier analysis of ARM and pseudo-Thellier analysis of TRM, *Earth Planet. Sci. Lett.*, *205*(3), 325–336.
Yu, Y., L. Tauxe, and B. M. Moskowitz (2004a), Temperature dependence of magnetic hysteresis, *Geochem. Geophys. Geosyst.*, *5*, Q06H11, doi:10.1029/2003GC000685.
Yu, Y., L. Tauxe, and A. Genevey (2004b), Toward an optimal geomagnetic field intensity determination technique, *Geochem. Geophys. Geosyst.*, *5*, Q02H07, doi:10.1029/2003GC000630.